SUSTAINABLE AND RESILIENT INFRASTRUCTURE
https://doi.org/10.1080/23789689.2019.1708182

Taylor & Francis
Taylor & Francis Group

A hybrid approach for transmission grid resilience assessment using reliability metrics and power system local network topology

Binghui Li[a], Dorcas Ofori-Boateng[b], Yulia R. Gel[b] and Jie Zhang[a]

[a]Department of Mechanical Engineering, The University of Texas at Dallas, Richardson, TX, USA; [b]Department of Mathematical Sciences, The University of Texas at Dallas, Richardson, TX, USA

ABSTRACT

Due to increasing threats on power systems from various extreme events such as adverse weather and cyber/physical attacks, research on power grid resilience is recently gaining a substantial traction. In this study, we evaluate the transmission grid resilience using the local topological summaries derived under a framework of topological data analysis (TDA) and more conventional power system reliability metrics. The dynamics of persistent topological features after an extreme event are examined to evaluate the impact on the underlying network structure. In addition, a framework based on an optimal power flow model is developed to investigate power system reliability metrics under extreme events. The developed methods are applied to a synthetic power system that is built on the footprint of the Texas power system. By comparing the TDA summaries with the power system reliability metrics, our findings show that local topological summaries can successfully reflect changes in the grid resilience.

ARTICLE HISTORY
Received 23 July 2019
Accepted 3 December 2019

KEYWORDS
Grid resilience; power system; graph theory; topological data analysis

1. Introduction

Power systems are critical infrastructures that are vulnerable to extreme events such as natural disasters, extreme weather, or pernicious human actions (National Academies of Sciences & Medicine, 2017). Due to its pivotal role in modern life, power system outages usually affect millions of people and pose great threats to everyday life, economic prosperity, and national security. The Northeast blackout of 2003 throughout parts of the Northeastern and Midwestern United States is estimated to affect at least 55 million people in Canada and the United States. The severe blackouts in India in 2012 affect over 600 million people or about 9% of the world population. In addition, growing evidence shows that the entire electricity supply chain, including generation, transmission, and distribution, is vulnerable to climate change (Chandramowli & Felder, 2014). Therefore, there exists a critical need to improve the resilience of power systems, such that major outages are less frequent, their impacts on society are reduced, and recovery is more rapid.

Resilience is defined as the capacity to anticipate, prepare for, respond to, and recover from significant disruptions (Sharma et al., 2018; Wilbanks & Kates, 2010). Due to its complex and interdisciplinary nature, previous studies have been conducted over a wide range of domains (Čaušević et al., 2019; Gasser et al., 2019; Wang et al., 2016). Graph theory and measures of complex network analysis have been applied to a variety of studies on the resilience of power systems (Ezzeldin & El-Dakhakhni, 2019). The electric power systems are often represented as networks/graphs, and the resilience and/or robustness of the power grid is then evaluated by assessing the dynamics of the topological properties of the graph, such as the node degree distribution, clustering coefficient, average path length, giant component size, etc. Holmgren (2006) examines the error and attack tolerance of the Nordic and the western United States transmission grids by scrutinizing the topological characteristics of the networks. Chassin and Posse (2005) develop a simple model to estimate the topology of the North American Eastern and Western power grids, which are combined with the scale-free network connectivity probability distribution to estimate the loss-of-load probability (LOLP). Chassin and Posse (2005) also compare the values of LOLP with other LOLP estimates previously obtained using standard power engineering methods. Ezzeldin and El-Dakhakhni (2019) scrutinize the robustness of the Ontario power network by evaluating several key network metrics. Guidotti et al. (2016) develop a unified methodology to model the network dependencies and interdependencies and incorporates the methodology in a six-step probabilistic procedure to assess the resilience of critical infrastructure. In several

CONTACT Jie Zhang jiezhang@utdallas.edu

studies (Cuadra et al., 2015; Pagani & Aiello, 2013; Rueda et al., 2017), a network with higher network robustness under extreme events is linked to higher clustering coefficient, lower average path length and/or higher mean degree. Furthermore, Wang et al. (2019) assess the structural robustness of the transmission network for central China by using percolation theory and the giant component size under random and deliberate node-based events. Percolation theory is based on quantifying the proportion of the network that is still connected after extreme events.

However, while assessment of grid resilience via these topological metrics reflects structural vulnerability under extreme events, it fails to reveal the grid dynamics that underlies power system operation. Historically, large-scale blackouts are triggered by simple faults, which evolve into cascading failure of other critical components due to violation of power system operation limits and eventually lead to catastrophic events (National Academies of Sciences & Medicine, 2017). Therefore, it is critical to examine the indicators related to power grid operation, such as reliability and security. Functionally, power system reliability is usually evaluated using metrics that reflect end-use demand satisfaction. Therefore, the power grid resilience characteristics are analyzed based on indicators that can measure system operating reliability. Liu et al. (2016) present a framework for analyzing the resilience of an electric power grid with integrated microgrids in extreme conditions by introducing several indices to measure the impact of extreme events. Trakas and Hatziargyriou (2017) utilize a stochastic program to improve the resilience of a distribution system exposed to an approaching wildfire. Ouyang and Duenas-Osorio (2014) conduct a resilience assessment of electric power systems to hurricanes by simulating the response of power systems based on a DC power flow model. Rocchetta et al. (2018) assess power system resilience by evaluating the expected energy not supplied using a vectorized emulator of the power flow solver to reduce the computational effort. The comparison between results from the emulator and the conventional more computationally expensive power flow method indicates similar accuracy. Similarly, Fang et al. (2014) simulate cascading failures in a network and quantify its resilience using a network-centric and a power flow model, where both models give similar results.

In this study, we evaluate the grid resilience using metrics from topological data analysis (TDA) and conventional power system reliability metrics. The interface of TDA encompasses algebraic topology, machine learning, statistics, and data science, and this offers a platform to systematically infer from the geometric structure and form of datasets. With the TDA-based metric, the transmission network is represented by an edge-weighted, undirected graph, and extreme events are represented by the removal of edges or nodes from the graph. The dynamics of persistent topological features after extreme events are examined and compared with the transmission network's original features. The motivation here is to capture the evolving structural dynamics (deformation) of the network due to the events. The structural deformation of the network is viewed as a proxy of the impact of the events on the network. In addition, we also develop a framework based on the optimal power flow (OPF) model and investigate conventional power system reliability metrics under extreme events. The developed framework is applied to a synthetic power system that is built on the footprint of the Texas power system. Insights are then drawn from the comparison between the topological metrics and the power system reliability metrics.

The contributions of this paper are twofold. First, the method of TDA is employed to examine the structural deformation of the graph representation of a real-world-sized transmission network. While traditionally many other graph characteristics are used, very few studies scrutinize the TDA summaries. In addition, the TDA summaries are compared against traditional reliability metrics of the transmission grid by examining their correlation coefficients, and their relations are further explained.

The paper is structured as follows: Section 2 details the methods used in TDA as well as the framework based on the OPF model. Section 3 gives an overview of the data used in our analysis. Section 4 presents the results and Section 5 concludes this paper.

2. Resilience quantification methodology

2.1. Graph representation of extreme events

A power transmission network typically consists of buses and branches. Buses may correspond to power generating plants and substations feeding demand. Branches may represent any series of devices in the network, such as transmission lines, transformers, or flexible alternating current transmission devices. The topological structure of a transmission network can be represented by a *graph G*, which is defined as a pair of sets of *nodes V* and *edges E*. Each element in the set of edges *E* represents a link between two nodes from the set *V*. Depending on whether edges have orientations or not, a graph can be *directed* or *undirected*. Therefore, a transmission network can be represented by a finite,

nonempty, undirected graph $G = (V, E)$, where the set of nodes V represents all buses and the set of edges E represents all branches in the transmission network. Note that although directed graphs are used in analyzing the actual flow of power in a network, we treat the transmission system as an undirected graph and the direction of power flow on a branch is determined by its sign. Figure 1(a) shows a simple 3-bus system with two generators and a load, which is represented by a graph with 3 nodes and 3 edges.

The above representation of a power transmission network assumes equally weighted edges. While this representation can capture the topological structure of a network, real-world power system performance is also measured with a diverse set of indicators, whose magnitude must be strictly limited within proper ranges. For example, the magnitude of power flow on a transmission line must be bounded by its thermal rating. Therefore, *weight* ρ can be assigned to edges in a graph to represent the characteristics associated with the edges and the graph becomes a *weighted* graph, which can be represented by $G = (V, E, \rho)$. Such weights may represent costs, lengths or capacities, depending on the problem at hand. For a transmission network, the weight of an edge can be a thermal rating of that edge.

Given the above graph representation of power transmission networks, an extreme event can be represented by the removal of a node, edge or a subgraph. An edge-based event represents the removal of one or more edges, which are commonly associated with line contingencies, such as tripping of a transmission line, or failure of transformers. By contrast, a node-based event represents bus-related contingencies, e.g., power plant outage or substation failure. Note that removal of a node also leads to the removal of all edges that are connected with the node, while removal of an edge does not affect its endpoints. As shown in Figure 1(b), the removal of transmission line between bus 1 and bus 2 results in a system with three buses but only two transmission lines, while in Figure 1(c), the removal of bus 2 also leads to failure of transmission line 1–2 and 3–2, resulting in a system with only two buses and one transmission line.

2.2. Topological data analysis in vulnerability analysis

Topological data analysis provides a mathematical foundation and systematic data science machinery for understanding the structure (shape) underlying the observed data. Therefore, TDA-based resilience metrics primarily reflect the structural response of transmission networks to various hazards. For instance, there is no direct relation between the number of p-dimensional holes detected by TDA and power system reliability. However, the TDA summaries can be employed to track changes within local topology and geometry of power systems under attacks and failures. Recently, several studies (Islambekov et al., 2018; Ofori-Boateng et al., 2019; n.d.) analyze power grid resilience under node- and edge-based

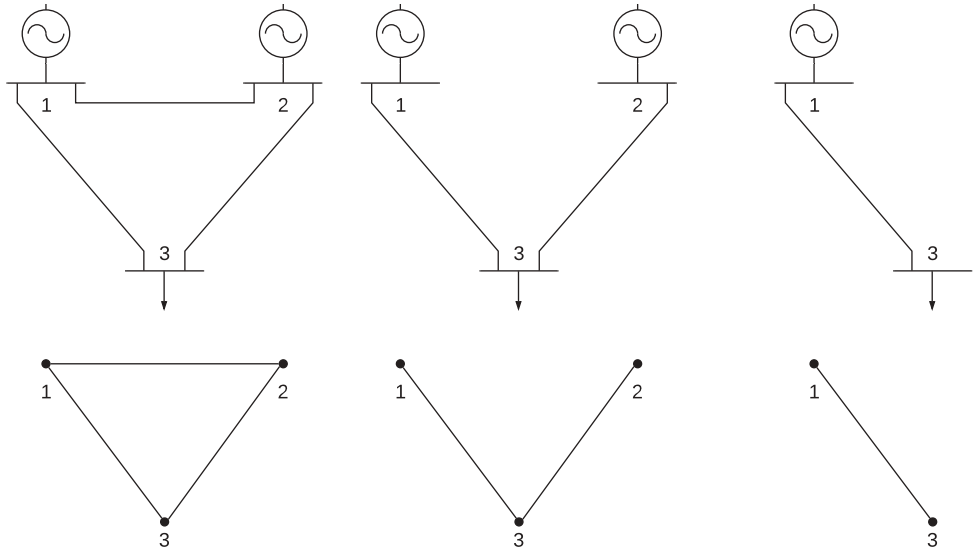

(a) The full graph. (b) Remove one edge. (c) Remove one node.

Figure 1. Graph representation of a 3-bus transmission network.

events via various *persistent homology* tools within the TDA framework, such as, for instance, the dynamics of Betti numbers and persistence diagrams.

Additionally, we postulate that a transmission network is more resilient if it is able to preserve most of its local topological structure after an event. In this study, our goal is to analyze the dynamics of persistent topological features under both node- and edge-based events following different removal strategies.

Let $G = (V, E, \rho)$ be an (edge)-weighted graph representing the given transmission network. For a specific threshold (or scale) $v_j > 0$ and for $u, v \in V(G)$, a subgraph G_j can be obtained by only keeping edges with weights $\rho_{uv} \leq v_j$. Therefore, the adjacency matrix $\mathbf{A}^j = (a^j_{uv})$ of G_j is defined as:

$$a^j_{uv} = \begin{cases} 1 & \text{if } (u,v) \in E \text{ and } \rho_{uv} \leq v_j \\ 0 & \text{otherwise.} \end{cases}$$

Next, we identify a simplicial complex (a finite collection of simplices) within each $G_j, j = 1, \ldots, n$. Basically, a k-simplex is the convex hull of $k+1$ points. Thus, a node is a 0-simplex, an edge is a 1-simplex, a triangle is a 2-simplex, etc. With simplicial complexes, we are able to (combinatorially) approximate the hidden geometry of a network. Given a sequence of n thresholds $v_1 < v_2 < \ldots < v_n$, we can obtain a hierarchically nested sequence of graphs $G_1 \subseteq G_2 \subseteq \ldots \subseteq G_n$. This procedure is known as a *network filtration*. In this study, the Vietoris-Rips (VR) filtration is used to extract topological features from the given transmission network due to its computational efficiency. For $v_j > 0$, the Vietoris-Rips complex is defined as $VR_j = \{\sigma \subset V | \rho_{uv} = d(u,v) \leq v_j, \forall u, v \in \sigma\}$, i.e., VR_j contains all the k-node subsets of G_j, $j = 1, \ldots, n$, which are pairwise connected by an edge as simplices of dimension $k-1$. Therefore, we obtain a sequence of VR complexes given a sequence of threshold v_j by applying VR filtration to a graph.

With the sequence of VR complexes $VR_1 \subseteq VR_2 \subseteq \ldots \subseteq VR_n$, we are able to determine the count of topological features in the form of *Betti numbers*. For a given simplicial complex, the pth Betti number (β_p) reflects the count of p-dimensional holes presented in the topological surface. For example, Betti-0 (β_0) gives the count of connected components and Betti-1 (β_1) corresponds to the count of one-dimensional holes (Delfinado & Edelsbrunner, 1995). By detecting the pth Betti number of each of the sequence of VR complexes, we obtain a n-dimensional vector of the pth Betti numbers $\beta_p = (\beta_{p,1}, \beta_{p,2}, \cdots, \beta_{p,n})$. The structural evolution of a transmission network under an extreme event can be evaluated using the relative change in the vector of Betti numbers defined as follows:

$$\Delta\beta_p = \frac{\| \beta_p - \beta_p^{'} \|_2}{\| \beta_p \|_2}$$

where $p = 0, 1$, and β_p and $\beta_p^{'}$ represent the vector of the pth Betti numbers for the original graph and the graph after an event, respectively (Islambekov et al., 2018).

In addition to the sequence of Betti numbers, the lifespan of topological features can be represented by *persistence diagrams* and *barcodes* (Carlsson, 2009; Ghrist, 2008; Kerber et al., 2016; Zomorodian, 2010). A persistence diagram is a multi-set of paired scale values corresponding to the birth and death times of topological features. In turn, persistence barcodes display the birth and death times of each topological feature with a horizontal bar. The (dis)similarity between persistence diagrams D_1 and D_2, which are extracted from graph G_1 and G_2, can be analyzed via a distance measure (Kerber et al., 2016; Otter et al., 2017). A commonly used distance measure is the Wasserstein distance (Wasserman, 2018), which is defined as

$$W_r(D_1, D_2) = \inf_{\gamma} \left(\sum_{x \in D_1} ||x - \gamma(x)||_\infty^r \right)^{1/r},$$

where $r \geq 1$, γ ranges over all bijections between D_1 and D_2, and $||z||_\infty = \max_i |z_i|$.

2.3. Power system reliability metrics

Resilience of a power network is defined as its capability to withstand system failure incurred by hazardous events, to reduce the impact of the events on customers, and to restore to normal operating status after the events. Grid resilience can be enhanced in a variety of ways, such as to build a system with sufficient redundancy (Wang et al., 2016). However, these measures usually come at additional costs. Although it is possible to design systems that can withstand all major failure events, the expenses of building and maintaining such systems can be prohibitively high. Therefore, an adequate reliability margin can serve as guidelines for the assessment of system resilience. Although there are myriad resilience metrics proposed (Willis & Loa, 2015), there are no generally agreed upon resilience metrics that are used widely, and most of the proposed metrics remain immature. Therefore, we follow traditional transmission reliability metrics to examine power grid resilience. Note that the concepts of reliability differ from resilience. While reliability metrics primarily evaluate resource adequacy and operating reliability, resilience is a broader concept that also accounts for the

power grid's capability to withstand random events, manage and ameliorate the consequences of an event once it occurs, and rapidly recover from an event.

Reliability metrics are grouped into those applied to generation and transmission systems and those for the distribution system (National Academies of Sciences & Medicine, 2017). We examine loss-of-load probability (LOLP) and expected unserved energy (EUE), two conventional reliability indices that are widely used in resource planning of generation and transmission systems (Allan et al., 2013; North American Electric Reliability Corporation, 2018). LOLP is defined as the probability of system daily peak or hourly demand exceeding the available generating capacity during a fixed period. Note that LOLP can be calculated by either using only the daily peak loads or all the hourly loads in each study period. During time $t \in T$, a loss-of-load event (I_t) occurs if total system load exceeds the maximum available system generating capacity:

$$I_t = \begin{cases} 0, & \text{if } \sum P_g^{max} \geq \sum_{b\in\mathbf{B}} L_b \\ 1, & \text{if } \sum P_g^{max} < \sum_{b\in\mathbf{B}} L_b \end{cases} \tag{1}$$

where P_g^{max} indicates the capacity of generator g and L_b denotes the load at bus b. The LOLP over the entire period T can be given by the following equation:

$$LOLP = \frac{1}{T}\sum_{t\in\mathbf{T}} I_t \tag{2}$$

Another reliability metric is EUE, which measures the summation of the expected number of megawatt hours of load that will not be served in a given time period. Different from LOLP, which only accounts for the duration of loss-of-load, EUE is an energy-centric measure that also considers the magnitude of loss-of-load. EUE can be either expressed in megawatt hours, or normalized based on the total number of megawatt hours of load:

$$EUE = \frac{\sum_{t\in\mathbf{T}} EUE_t}{\sum_{t\in\mathbf{T}} L_t} \tag{3}$$

where EUE_t represents the energy that is not supplied and L_t denotes the load during time t. Therefore, the normalized EUE is a dimensionless scalar that ranges from 0 to 1.

While LOLP and EUE can be used to measure resource adequacy in resource planning, daily power network operation is also subject to a wide range of constraints that are not considered in resource planning, such as power flow limits, bounds of voltage levels and phase angles. Such operating schedules are typically determined by solving OPF models, which are formulated as a mathematical program aiming at minimizing the total production cost or transmission loss by optimizing dispatch and control settings of power systems. This type of problem underlies a diverse set of applications in modern power system engineering, such as economic dispatch, unit commitment, state estimation, stability and reliability assessment (Wood & Wollenberg, 2012). The OPF problem explicitly enforces security constraints to meet the physical operating limits of the power network. While the OPF problem can determine dispatch settings during normal operation, network contingencies may lead to infeasibility under extreme events. Therefore, we develop a relaxed OPF model by adding slack variables to the load balance constraint, which are activated when a limited supply is present due to contingency. A penalizing cost is also added to the objective function to prevent the slack variables from being activated at normal operating status. The complete model formulation is given below.

$$\min \sum_{g\in\mathbf{G}} F_g(P_g) + \sum_{b\in\mathbf{B}} M \cdot S_b \tag{4a}$$

$$\text{s.t.} \quad B\theta = C_g P - L + S, \tag{4b}$$

$$P_g^{min} \leq P_g \leq P_g^{max}, \forall g \in \mathbf{G}, \tag{4c}$$

$$\theta_b^{min} \leq \theta_b \leq \theta_b^{max}, \forall b \in \mathbf{B}, \tag{4d}$$

$$S_b \geq 0, \forall b \in \mathbf{B}. \tag{4e}$$

where function $F_g()$ is the cost function for generator $g \in \mathbf{G}$, and M is the penalty cost for slack variable S_b, which is introduced in (4b) to denote shedded load at bus $b \in \mathbf{B}$. The cost functions are typically modeled in a convex form, e.g., quadratic or piecewise linear functions, to ensure global optimality. The relaxed load balance constraint is enforced in (4b), where B is the imaginary part of system admittance matrix, C_g is the generator connection matrix, L is the vector of load at each bus, and S is a vector of slack variables S_b. Constraints (4c) and (4d) together limit dispatch setting points within system tolerances. Finally, constraint (4e) ensures the shedded load must be non-negative.

The relaxed load balance constraint in (4b) implies that load shedding can be determined by examining the slack variable S_b. Under optimality conditions, a positive S_b indicates the shedded load at bus b, which implies the occurrence of loss-of-load. Therefore, the criterion of the occurrence of a loss-of-load event in (1) becomes:

$$I_t = \begin{cases} 0, & \text{if } \sum_{b\in\mathbf{B}} S_b = 0 \\ 1, & \text{if } \sum_{b\in\mathbf{B}} S_b > 0 \end{cases} \tag{5}$$

In addition, the *EUE* during time t can also be given by the slack variable S_b:

$$EUE_t = \sum_{b \in \mathbf{B}} S_b \tag{6}$$

2.4. Reliability analysis framework

Due to the unpredictability of random events, a critical rule in the U.S. is the NERC $(n-1)$ rule, which specifies that the grid shall continue to operate in the Normal State following the loss of one generating unit, transmission line, or transformer (Wood & Wollenberg, 2012). The rationale behind is that the initial outage of one component could result in violations on other components, which further lead to cascading outages. Therefore, the $(n-1)$ rule ensures no single component outage will result in other component outages.

While the $(n-1)$ contingency analysis assesses system reliability under single component outage, random hazardous events such as a storm may cover a large area, which could lead to outages of more than one component. Therefore, it is desirable to examine system reliability when outages happen to more than one component. As described in Section 2.1, an extreme event is simulated by randomly removing one or more nodes or edges. In this study, we examine the topological and reliability metrics defined in the previous sections after multiple network components are removed. In addition, another motivation of this study is to identify the critical components of which removal will lead to a greater impact on the grid resilience. This analysis is conducted by scrutinizing the changes in the metrics to the number of removed components. For example, when an equal number of nodes are removed, a greater EUE indicates that the removed nodes play a greater role in the grid resilience in terms of unserved energy.

A significant number of studies have been conducted to analyze grid resilience by examining topological summaries when network components are removed (Albert et al., 2004; Chassin & Posse, 2005; Holmgren, 2006; Kim et al., 2017; Rosato et al., 2007). Most studies assume the network components are removed following a fixed order based on a selected attribute of the components. The selected attribute can be topological summaries of the nodes or edges, such as degrees of nodes, or engineering parameters, such as thermal ratings of transmission lines, or rated voltage levels of substations. In our study, the network components are removed in two ways: random removal, where the nodes or edges are removed in a totally random order, and ordered removal, where the network components are ranked based on one of their attributes, and then removed following the rank. We use the random removal as a baseline, which reflects the intrinsic grid resilience against natural events. By contrast, the ordered removal reflects how the selected attribute is related to grid resilience, i.e., by comparatively examining the response of resilience metrics when network components are removed following the order of different attributes, one can identify the most critical one and enhance grid resilience by applying protective measures.

The selected attributes used in this study are tabulated in Table 1. We examine both thermal rating of transmission lines and degree of nodes. In graph theory, the *degree* of a node is the number of edges connecting to the node and a node of greater degree may represent a substation that is connected with more transmission lines. Typically, a transmission hub plays important roles in the power grid, which may further imply greater importance in grid resilience.

Therefore, for each ordered removal, we define a sequence of nodes or edges that follow descending orders of a given attribute. For nodes, an ordered sequence can be expressed by:

$$v_1, v_2, \cdots, v_i, \cdots, v_{N_V}$$

where $v_i \in V, N_V = |V|$, and the selected attribute a_i associated with node v_i satisfies the following inequalities:

$$a_1 \geq a_2 \cdots \geq a_i \geq \cdots \geq a_{N_V}$$

Similarly, for edges a sequence can also be given:

$$(u_1, v_1), (u_2, v_2), \cdots, (u_j, v_j), \cdots, (u_{N_E}, v_{N_E})$$

where $(u_j, v_j) \in E, N_E = |E|$, and the selected attribute b_j associated with edge (u_j, v_j) satisfies the following inequalities:

$$b_1 \geq b_2 \cdots \geq b_j \geq \cdots \geq b_{N_E}$$

For an event where k edges/nodes are removed, the first k elements from the given sequence are removed. Then, the power grid after the event is represented by the subgraph consisting of the remaining nodes and edges.

After an event, a power grid may be split into several isolated grids, which are also known as islands. An island is a subset of components of the original network that is isolated from the original network. Since there is

Table 1. The attributes by which edges/nodes are ordered.

Attribute		Notes
Edge	Random	Random removal
	MVA	Thermal ratings of transmission lines.
	sumDegree	Sum of degrees of end nodes.
Node	Random	Random removal
	sumMVA	Sum of thermal ratings of connected lines.
	Degree	Degree of the node.

no interconnection between isolated islands, each island can be viewed as an independent power network. In addition, since an island only includes a subset of components from the original network, it is more likely to be vulnerable to contingencies. Mathematically, a graph is called disconnected if it can be partitioned into at least two subsets of nodes such that there is no edge connecting them. Therefore, the number of isolated islands is determined by examining the number of subgraphs after an event. In this study, if the original power grid is split into multiple islands, we examine the occurrence of loss-of-load ($I_{t,d}$) and EUE of each island separately. The system EUE is then calculated by summing up EUEs of all islands, and the system LOLP is given by Equation (7).

$$I_t = \begin{cases} 0, & \text{if } I_{t,d} = 0, \forall d = 1, \cdots, D \\ 1, & \text{otherwise} \end{cases} \tag{7}$$

where D denotes the number of isolated islands. The system LOLP can then be derived by examining all $I_{t,d}$ over the entire time periods using Equation (2).

One challenge in simulating random events that involve multiple components is to determine the components that are removed. If k nodes/edges are to be removed from a graph, there are $k!$ ways to randomly select the k components, which approaches infinity as k increases. In addition, in the ordered removal, the selected attributes such as thermal ratings of transmission lines may see identical values shared by many components:

$$a_1 \geq a_2 \cdots \geq a_i \geq a_{i+1} = \cdots = a_{i+m} \geq \cdots \geq a_{N_V} \tag{8}$$

Suppose $i < k < i + m$, then there are at least $\binom{m}{k-i}$ ways to determine a sequence that includes k removed components. Although ideally each possible sequence should be examined, it is computationally prohibitive to examine all of them as k increases, given that a real-world -sized network usually has more than thousands of edges and nodes. Therefore, without loss of generosity, we repeat our experiments multiple times for the random removal as well as the ordered removals. For the random removal, the number of experiments are 50, while for the ordered removal, the number is given by the smaller value between $\binom{m}{k-i}$ and 50. The repeated experiments are intended to give a comprehensive evaluation of all possible events and produce robust results.

The above framework of this study is summarized in Algorithm 2 where nodes are removed in an ordered sequence. Edge-based events can be simulated in a similar fashion. Note that we use 1 year's daily peak load to represent 1 year's load for simplicity. The implementation of our method is coded in MATLAB and we use MATPOWER (Zimmerman et al., 2010), a free and open-source MATLAB package, to solve the DC-OPF model. A high-performance computing platform equipped with a 20-core Xeon E5-2698 CPU and 256 GB of memory is used, where the model can be parallelized for better time performance.

Algorithm 1 Analysis framework

procedure GRID RESILIENCE ANALYSIS
  Initialize node sequence $(v_1, \cdots, v_{N_V})$
  for $k = k_1, \cdots, K$ **do** Remove k nodes:
    Remove nodes $v_1, \cdots, v_k$
    $D \leftarrow$ number of islands
    for $d = 1, \cdots, D$ **do** Yearly simulation
      for $t = 1, \cdots, T$ **do** DC-OPF
        Calculate $I_{t,d}$ and $EUE_{t,d}$
      end for
    end for
    Calculate *LOLP* and *EUE*
  end for
end procedure

3. Data

A critical motivation of this study is to apply the proposed method to real-world power systems. However, due to confidentiality requirements on critical infrastructure information, data availability of real-world power systems is usually limited. Therefore, to simulate real-world power system operation, we use a well-developed, publicly available synthetic network developed by Birchfield et al. (Birchfield et al., 2017). Note that although this test case is entirely fictitious, it shares significant similarities with real-world power systems in terms of statistical characteristics found in actual grids.

Modern power system networks are complex interconnected networks, which can be divided into four subnetworks: generation, transmission, distribution, and loads. This study focuses only on the transmission network, which bridges the generators and distribution systems via substations. Transmission networks are often operated at tens or even hundreds of kilovolts to reduce transmission loss over long distances. The transmission network used in this study is built on the footprint of the Electric Reliability Council of Texas (ERCOT), which is the independent transmission operator that serves most of the Texas territory. By synthesizing public information on population and generating plants at postal code level, the Texas system places 2,000 buses. Each bus may be connected to a load,

a generator or both. The 2,000 buses are connected by 3,206 transmission lines, which can be reduced to 2,667 unique edges since one edge may include multiple transmission lines. Therefore, the Texas power grid network is represented by a graph with 2,000 nodes and 2,667 edges.

We use 1 year's daily peak load to conduct the reliability assessment. The hourly load in 2017 is drawn from ERCOT and rescaled by multiplying a scaling factor such that the maximum load does not exceed the synthetic network's total generating capacity. The scaling factor is calculated by dividing the given total load from the synthetic network by the maximum hourly load in 2017 from ERCOT. We assume a fixed load distribution factor in order to calculate the load on each bus. Note that although one plain year consists of 8760 h, we only consider 365 daily peak loads and use the 365-h load profile to represent the yearly load profile.

4. Results

4.1. TDA summaries

The changes in the topological summaries are displayed in Figures 2 and 3. Three metrics are examined: $\Delta\beta_0$, $\Delta\beta_1$, and Wasserstein distances. Overall, all three summaries exhibit increasing trends, indicating greater structural deformation when more nodes or edges are removed. For example, in the random removal, $\Delta\beta_0$ increases from less than 1% when 10 edges are removed to over 3% when 100 edges are removed and $\Delta\beta_1$ rises from around 2% to over 10% over the same range, as shown in Figure 2(a,b). Meanwhile, Figure 3(a,b) indicates that the random node removal sees similar yet faster increasing trends than the random edge-based removal: $\Delta\beta_0$ and $\Delta\beta_1$ rise to 4% and 12% when 60 nodes are removed, as opposed to 2% and 7% when the same number of edges are removed.

Despite similar increasing trends, significant differences are also presented across our results. The magnitude of the increasing trends varies noticeably with the removal strategies and the topological summaries in the edge-based events. For example, as indicated in Figure 2(a), the highest $\Delta\beta_0$ is presented when edges are removed following the order of the sum of degrees: it increases to over 4% when 100 edges are removed. By contrast, Figure 2(b) shows removing 100 edges following the same order results in the smallest $\Delta\beta_1$ value across all three removal strategies.

The node-based events, however, see more consistent increasing trends across the three removal strategies:

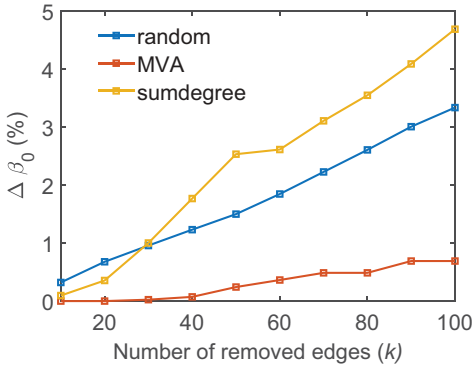

(a) Relative change in β_0.

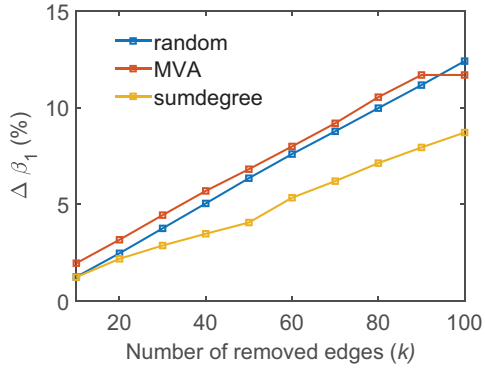

(b) Relative change in β_1.

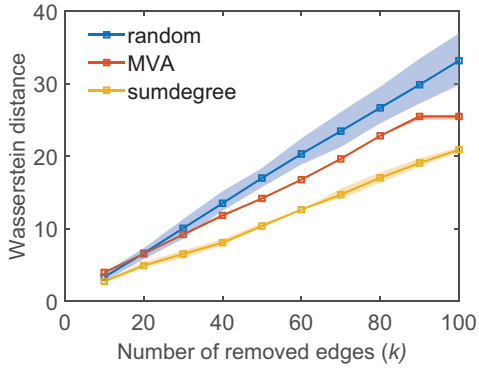

(c) Wasserstein distance.

Figure 2. TDA summaries under edge-based events. Note that the colored bands represent 90% confidence intervals.

Unlike in the edge-based events where ordered removals may see lower $\Delta\beta_0$ and $\Delta\beta_1$ than the random removal, the random removal always exhibits the lowest $\Delta\beta_0$ and $\Delta\beta_1$ when nodes are removed, as shown in Figure 3(a,b). In addition, when nodes are removed following the order of degree values, $\Delta\beta_0$ and $\Delta\beta_1$ values are always the highest, indicating the greatest structural deformation.

While the Betti numbers only reflect the number of k-dimensional holes, the Wasserstein distance gives a comprehensive and robust evaluation of structural deformation by neglecting short-lived topological features on the persistence diagrams. Figure 2(c) shows that the random removal still sees the highest increase of the Wasserstein distance when edges are removed. By contrast, Figure 3(c) shows that the random removal results in the lowest increase of the Wasserstein distance. In addition, the node-based removals present greater changes in the Wasserstein distance than the edge-based removals: when 60 edges are randomly removed, the Wasserstein distance increases to 20, while when the same number of nodes are randomly removed, the Wasserstein distance increases to 30. Therefore, our results suggest that when the same number of nodes or edges are removed, the node-based removal leads to greater deformation of network topological structure, due to the fact that removal of one node can also lead to the removal of one or more edges connected with the node. Besides, the differences of trends across the studied topological summaries indicate that each topological summary characterizes the structural deformation from a different perspective.

4.2. Reliability metrics

While the TDA summaries reflect structural changes in a network, power grid reliability is usually measured by metrics that reflect how the load is met by supply. Figures 4 and 5 illustrate how the removal of network components can affect grid reliability by a single case study. In both cases, a fixed number of nodes or edges are removed from the original network, and their impact on grid resilience is evaluated using the magnitude of the unserved load. In Figure 4, the total load and total served load after 80 edges are removed are presented. Since removing edges only affects transmission

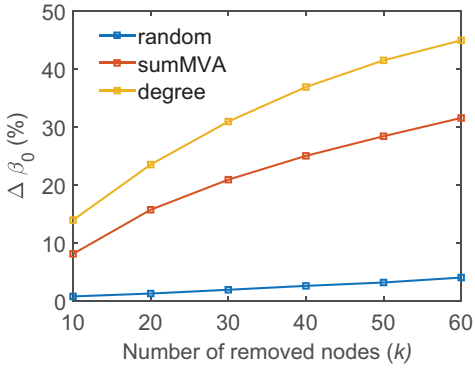

(a) Relative change in β_0.

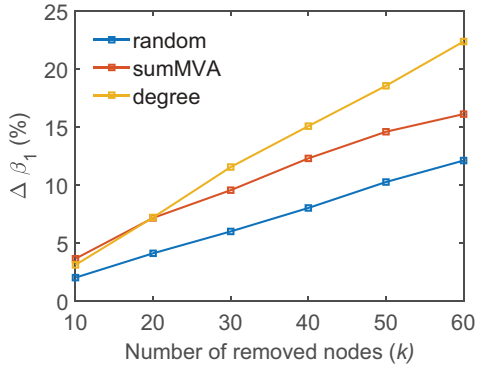

(b) Relative change in β_1.

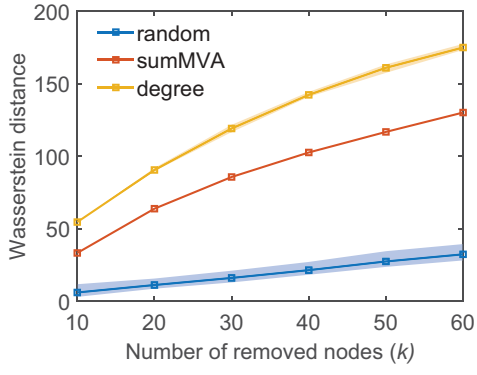

(c) Wasserstein distance.

Figure 3. TDA summaries under node-based events. Note that the colored bands represent 90% confidence intervals.

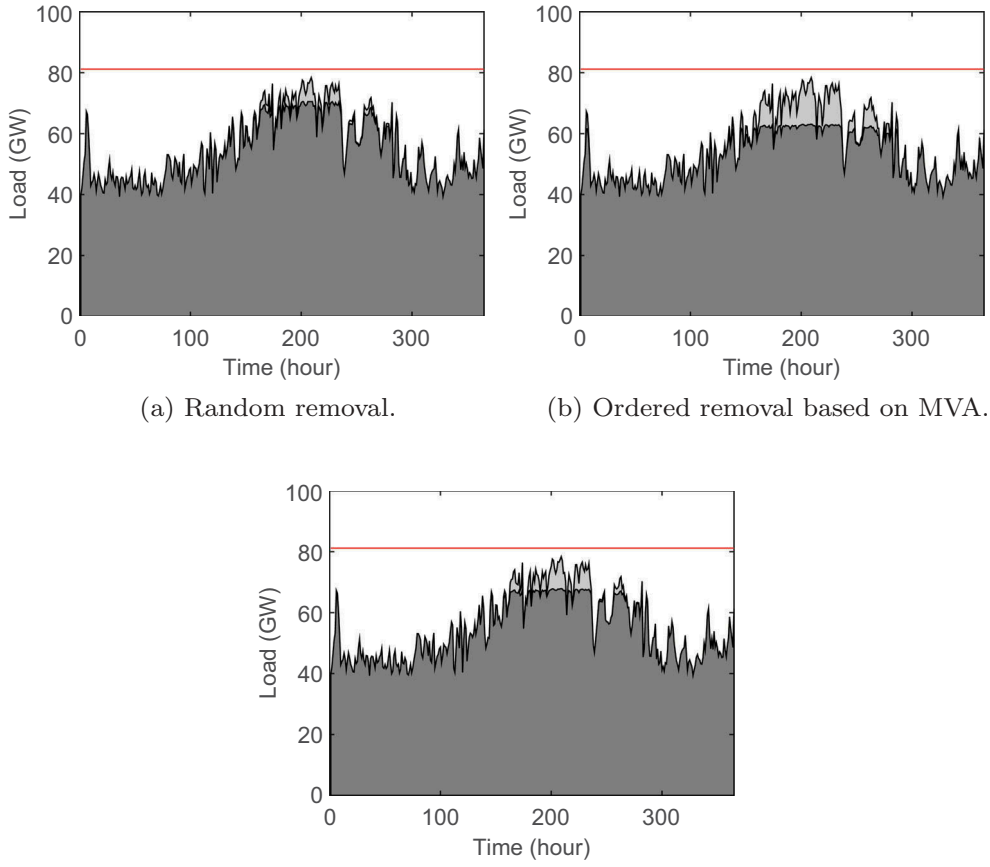

(a) Random removal.

(b) Ordered removal based on MVA.

(c) Ordered removal based on sum of degrees.

Figure 4. Time series of daily peak load and served load after 80 edges are removed. Upper edges of the light shaded areas represent daily peak load in a year, and lower edges of the light shaded areas represent served load. Therefore, the light shaded areas in between represent the megawatt hour values of the unserved load. The horizontal red lines represent total capacities remaining in the grid after the event.

lines or transformers, connections between generators and substations remain intact and the total generating capacities stay the same. Therefore, the total capacities are 81 GW across all three cases, enough to supply the peak load over the studied period. However, although the grid has sufficient generating capacities, outages of transmission lines may cause loss-of-load due to transmission congestion. For example, the total unserved energy in the random removal case (Figure 4(a)) amounts to 350 GWh or 1.7% of the total yearly load. In addition, ordered removals result in greater loss of load: the total amount of unserved energy is 914 GWh, or 4.5% of total yearly load, when the edges are removed following the order of MVA values, and 420 GWh (2.1%) following the order of the sum of degree values. This suggests that it can cause a greater loss of the load by removing edges with higher thermal ratings or higher sum of degree values.

In Figure 5(a), when 20 nodes are removed randomly, the total available capacity drops from 81 GW to 70 GW, resulting in 212 GWh (1%) of loss of load. In addition, although the losses of total generating capacity in the two ordered removals are slightly less than the random removal, the unserved load in both cases are significantly higher: it sees 4,000 GWh (20%) and 3,000 GWh (14%) of total unserved energy when the nodes are ordered by the sum of MVA and degree values, respectively. Unlike the removal of edges, the removal of nodes can further result in the failure of all edges connected with the removed nodes. Therefore, removal of one node often leads to loss of multiple edges. In addition, extreme events occur to a node can also result in the loss of all connected generators and exacerbate the situation. This implies that when an equal number of nodes and edges are removed from the same network, the node-based removal can result in greater losses in terms of unserved end-use load. This is proved in the presented results by the fact that the unserved energy from the case when only 20 nodes are removed is considerably higher than the case when 80 edges are removed.

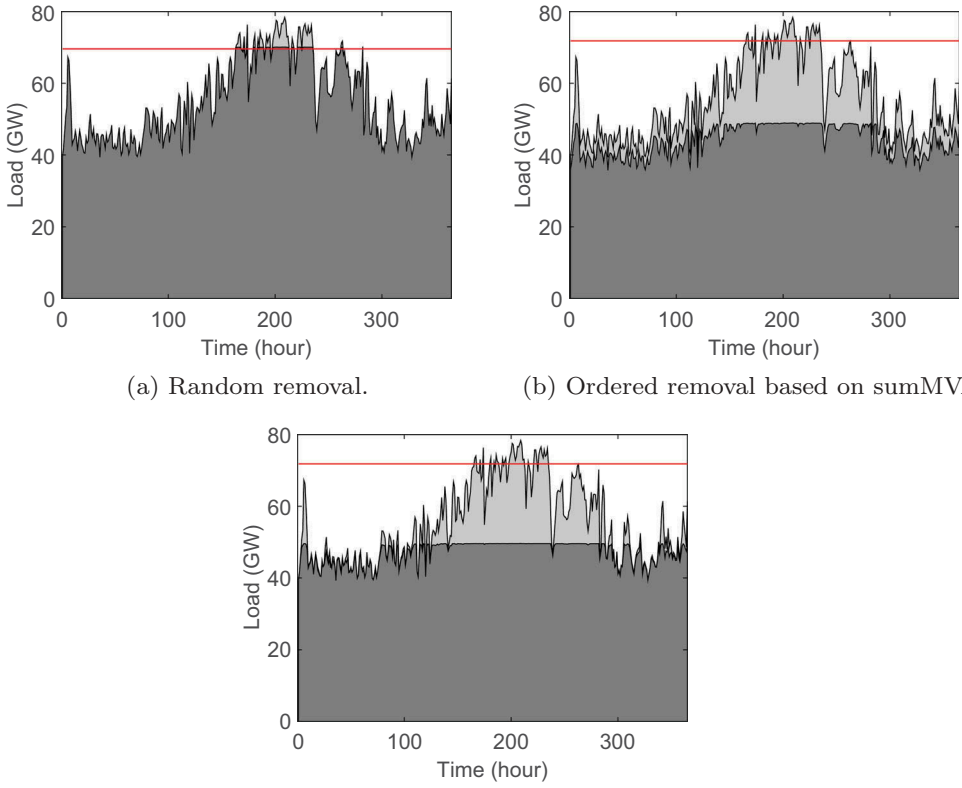

(a) Random removal.

(b) Ordered removal based on sumMVA.

(c) Ordered removal based on degree.

Figure 5. Time series of daily peak load and served load after 20 nodes are removed. Upper edges of the light shaded areas represent daily peak load in a year, and lower edges of the light shaded areas represent served load. Therefore, the light shaded areas represent the megawatt hour values of an unserved load. The horizontal red lines represent total capacities remaining in the grid after the event.

4.3. Dynamic changes in reliability metrics

The results presented above only show the unserved energy when a fixed number of network components are removed. To compare the grid reliability metrics when an increasing number of network components are removed, the simulation is repeated over a range of numbers of removed components. Due to greater impact from node-based events on the grid when equal numbers of components are removed, the number of removed nodes ranges from 10 to 60, while the number of removed edges ranges from 10 to 100.

The results from the edge-based events are illustrated in Figure 6. Figure 6(a) shows both the medians and variations of LOLP as a function of the number of removed edges in the random removal. The median LOLP increases from around 0.3 to 1.0 as the number of removed edges increase from 10 to 100. The increasing trend of the median suggests a greater risk of loss-of-load as more edges are removed. The 50% confidence intervals, as represented by the heights of blue boxes, range from 0.1 when $k = 10$ to over 0.5 when $k = 40$, indicating great uncertainties due to the random nature of the removal. In Figure 6(b,c), both the mean LOLP and mean EUE present increasing trends in the random removal: the mean LOLP rises from around 0.4 when $k = 10$ to 0.9 when $k = 100$, and the mean EUE rises from around 0.01 to 0.02 over the same range of k.

Figure 6 also shows results from the two ordered removals, where the edges are ordered by MVA ratings and sum of degree values. Comparing with the results from the random events, both ordered removals show significantly less uncertainties. The two ordered removals in the edge-based events result in lower mean LOLP than the random removal. This is consistent with the results presented by the Wasserstein distance in Figure 2(c), where the random removal results in the greatest deformation of topological structure.

Nevertheless, although the two ordered removals exhibit lower risk of loss-of-load, the unserved energies in both cases are higher: as shown in Figure 6(c), the mean EUE in the random removal rises to only 2% when 100 edges are removed, while the mean EUE surges to 7% when edges are removed following the order of MVA values. This indicates that even though the random removal shows greater mean probabilities of loss-of-load, the impact on electricity supply is less severe than the ordered removals. In particular, the mean unserved energy when edges are removed by following the order of

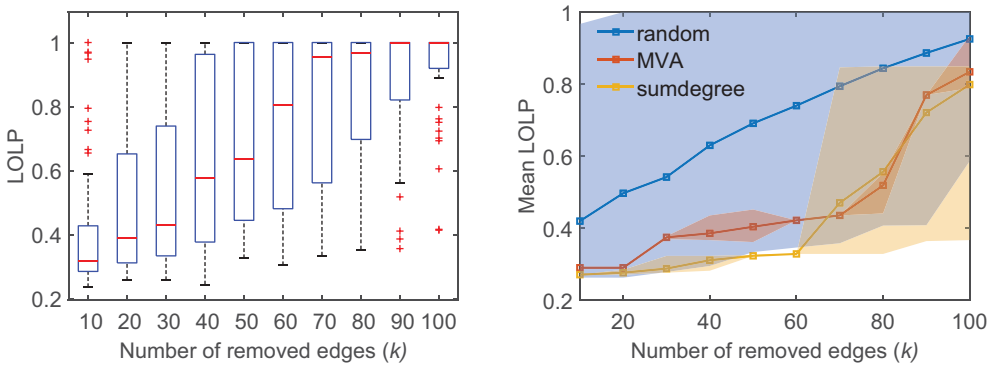

(a) LOLP in the random events. (b) Mean LOLP of different events.

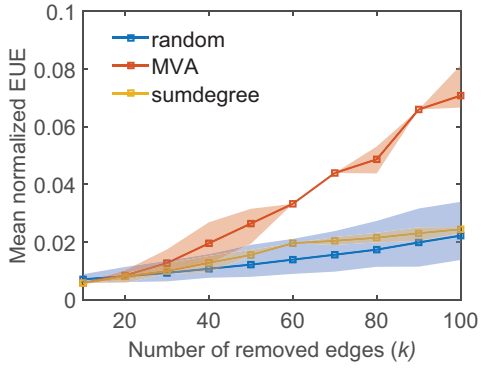

(c) Mean EUE.

Figure 6. Reliability metrics from the edge-based events. Note that in (b) and (c) the colored bands represent 90% confidence intervals.

MVA ratings is considerably greater than the other two cases: around 8% of total annual electric demand is unserved when 100 edges with the greatest MVA ratings are removed, while the other two removals only lead to less than 3% of unserved energy. This is possibly due to the pivotal role of the transmission lines with greater MVA ratings in the transmission grid resilience.

In addition, the random removal presents significant greater uncertainties associated with LOLP. As shown in Figure 6(b), the widths of the 90% confidence intervals of the random removal are greater than 0.7, while in the ordered removals the widths are less than 0.5. Furthermore, the uncertainties associated with EUE are significantly lower than LOLP, as shown in Figure 6(c), the widths of the 90% confidence intervals of the random removal are less than 0.02 most of the time. This indicates that the LOLP is a less robust evaluation metric of grid reliability than the EUE when the edges are randomly removed.

The results from the node-based events are presented in Figure 7. Note the number of removed nodes spans 10 to 60. Similar to the random edge-based events, the LOLP in the random removal also scatters over dispersed ranges, especially when the number of removed nodes ranges from 30 to 50, as depicted in Figure 7(a). The median LOLP increases from around 0.3 to 0.9 as the number of removed nodes increases from 10 to 60. Likewise, the increasing trend of the median suggests a greater risk of loss-of-load as more nodes is removed.

However, unlike in the edge-base events where the random removal presents the highest mean LOLP, both ordered removals exhibit a significant greater mean LOLP than the random removal, as shown in Figure 7(b). For example, the mean LOLP in the random removal starts at 0.4 when $k = 10$ and rises to 0.8 when $k = 60$. By contrast, the mean LOLP roared to 1 when $k = 20$ and stays constant thereafter in both ordered removals. These results imply that the grid is likely to suffer from a 100% chance of loss-of-load even only 20 nodes are lost in the two ordered removals.

As presented in Figure 7(c), the mean EUE values follow a similar increasing trend as the mean LOLP shows. In the random removal, although the mean LOLP rises to over 0.8 when 60 nodes are removed, the rise of the mean EUE value is marginal: it reaches 0.02 when $k = 60$, only slightly higher than 0.01 when 10 nodes are removed. Therefore, similar to the edge-based removal, even though there are great chances of loss-of-load in the random removal, the magnitude of each loss-of-load event is small. By contrast, the two ordered removals present

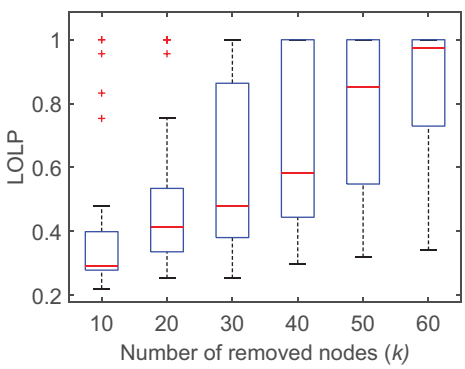

(a) LOLP in the random events.

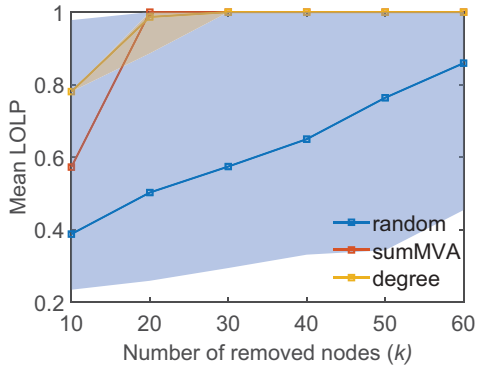

(b) Mean LOLP of different events.

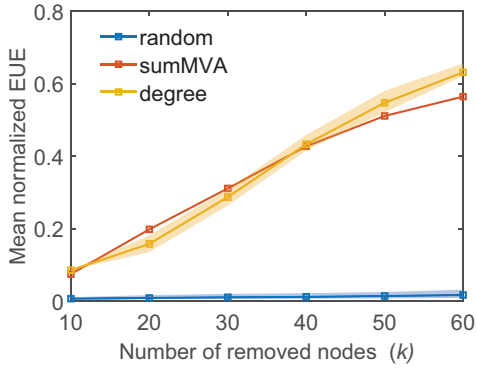

(c) Mean EUE.

Figure 7. Reliability metrics from the node-based events. Note that in (b) and (c) the colored bands represent 90% confidence intervals.

considerably higher unserved electric demand: the mean EUE increases from less than 0.1 at $k = 10$ to over 0.6 at $k = 60$ in both ordered removals, indicating a significant impact on the power system reliability.

Similar great uncertainties associated with LOLP are observed for the random removal, while both ordered removals present narrower 90% confidence intervals. In addition, Figure 7(c) also presents more concentrated results of EUE than LOLP. This further implies that EUE is a more robust metric than LOLP in terms of grid reliability.

In order to examine the relations between the TDA summaries and reliability metrics, the correlation coefficients are adopted. As demonstrated in Tables 2 and 3, the coefficients vary with the removal strategy and the metrics. Generally, the EUE exhibits a stronger correlation with the TDA summaries than the LOLP does, especially in the node-based removals. This is probably due to the fact that the LOLPs soon hit the upper bound of 1 in the ordered node-based removals. In addition, while the EUE is strongly correlated with all TDA summaries, the correlation is slightly stronger with Betti-1 in the edge-based removal, and with the Wasserstein distance in the node-based removal.

Table 2. Mean correlation coefficients between the TDA summaries and reliability metrics from the edge-based events.

	LOLP	EUE
Betti-0	0.930	0.974
Betti-1	0.966	0.992
Wasserstein distance	0.971	0.993

Table 3. Mean correlation coefficients between the TDA summaries and reliability metrics from the node-based events.

	LOLP	EUE
Betti-0	0.849	0.989
Betti-1	0.808	0.995
Wasserstein distance	0.845	0.990

5. Conclusion and discussion

In this study, the concept of TDA, specifically persistent homology, is employed to analyze the grid resilience of regional transmission networks. The transmission network is represented as an edge-weighted, undirected graph, while extreme events are simulated by removals of nodes or edges. By examining the changes of three TDA summaries under extreme events, we demonstrate how the network topological structure is affected by

extreme events. In addition, we also investigate the conventional reliability metrics used in resource planning studies, which reflect grid resilience from the end-use demand satisfaction perspective.

As demonstrated in the results, both the TDA summaries and power system reliability metrics suggest that an increased number of removed components leads to the deterioration of grid resilience. However, the evaluated indicators differ significantly when different removal strategies are adopted. For example, random removal results in the highest risk of loss-of-load (measured by LOLP) and Wasserstein distances when edges are removed, whereas it leads to the lowest LOLP and Wasserstein distances when nodes are removed. In addition, both ordered removals lead to greater impact than the random removal in terms of unserved energy.

Although all three TDA summaries reflect structural deformation of the transmission network, the results differ significantly with removal strategies, especially under the edge-based events. The inconsistency in the results can be attributed to the difference in the information conveyed by the three TDA summaries. For example, during the network filtration process, the pth Betti number only accounts for the number of p-dimensional holes in each subgraph, while a persistence diagram also records the birth and death times of each persistent topological feature. In addition, the framework of persistence diagrams is able to distinguish between persistent features and topological noises by neglecting short-lived features. Since long-lived motifs are more likely to play an important role in network functionality, the Wasserstein distance gives a more robust evaluation of the changes in network functionality. Therefore, greater changes in the persistent topological features indicate greater impact on the network functionality, which can lead to higher LOLP. As Figure 2(c) shows, the random removal suggests the greatest changes in the network's topological structure, which agree well with the highest risk of loss-of-load displayed in Figure 6(b). Similarly, Figures 3(c) and 7(b) indicate that the random removal exhibits the lowest Wasserstein distances and LOLPs among all three removal strategies.

Second, our study not only considers resource adequacy, i.e., the total available system capacity must exceed peak load, but also system security, i.e., flow limits on transmission lines. As demonstrated in Figure 4, although all generating units remain intact and the system has enough capacity after edges are removed, loss-of-load can still occur due to loss of transmission capacities. Further examination of Figures 6(c) and 7(c) indicate that removal of edges with higher MVA ratings or nodes with higher sum of MVA ratings leads to substantially greater unserved energy, since extreme events occur to these edges or nodes can considerably reduce the overall transmission capacity of the transmission network, and lead to significantly greater unserved energy due to transmission congestion.

Several caveats exist in our analysis. First, the DC-OPF model in our analysis only determines the setting points of all thermal units without considering unit commitment (UC) constraints. In real-world operations, operation of thermal units is subject to a diverse set of constraints that include minimum on-line time, ramp rates and start-up and shut-down time (Carrión & Arroyo, 2006). In order to determine the unit commitment statuses of thermal units, real-world power market operating schedules are typically determined based on power market simulations over time scales that range from day-ahead to real-time on a cost-minimization basis. Different from the OPF model, which is modeled as a continuous optimization problem, UC models are typically modeled as mixed integer programs, which are significantly more challenging to solve. In this analysis, we assume all units are online and there are no minimum online power constraints. Since we only consider 1 hour per day, it is realistic to neglect constraints on unit start-up and shut-down. However, it can inspire further research directions by considering how random events may influence multi-timescale market scheduling and operation.

Another caveat is that the post-event restoration is not taken into account by using the measure of reliability. Typically, the exact steps and procedures for restoration vary depending on the nature of the outage and the damage incurred. While the real-world recovery process can be simulated using the empirical model (Ji et al., 2016) or random process (Liu et al., 2016), this study does not follow such paths due to the complexity introduced by the lack of specific types or characteristics of the events.

In addition, the OPF problem in Equation 4 is formulated with DC power flow constraints (DC-OPF) as opposed to the complete AC form, which is also known as the AC-OPF problem (Wood & Wollenberg, 2012). The simplified DC-OPF model only includes active power flow terms and drops the reactive power flow terms, which results in a set of completely linear power flow constraints and fits in the field of linear or quadratic programming. The DC-OPF model is adopted since global optimality is guaranteed due to convexity. By contrast, the full AC-OPF problem is modeled as a quadratically constrained quadratic programming (QCQP) problem and the feasibility region is typically a non-convex set. While

convex QCQP problems can be solved efficiently, it is extremely challenging to solve non-convex QCQP problems (Calafiore & El Ghaoui, 2014). While the accuracy of DC-OPF approximation is questionable in distribution networks, it does not cause systematic errors in large-scale transmission networks, such as the one in this analysis.

Last, the developed analytical framework is only applied to the synthetic power grid of Texas, which may limit the generalization of our findings to different transmission networks. While the primary goal of this study is focused on the method and we only use one transmission network for demonstration purpose, the soundness of our study can benefit largely by extending it to larger power systems with drastically different topological characteristics, and further insights can be drawn from comparative studies across different power systems.

Disclosure statement

No potential conflict of interest was reported by the authors.

Funding

Gel is partially supported by NSF DMS [1736368]; NSF ECCS [1824716]; and NSF IIS 1633331.

Notes on contributors

Binghui Li received his Ph.D. in Civil Engineering from North Carolina State University in 2018. He is currently working as a postdoctoral research associate at the University of Texas at Dallas. His research interests are in the fields of energy system analysis, stochastic programming, and electricity markets.

Dorcas Ofori-Boateng is presently a Ph.D candidate in Statistics, under the supervision of Professor Yulia R. Gel, at the University of Texas at Dallas. Her research interests are associated with statistical foundations of data science, topological data analysis and anomaly detection in application to power systems, fMRI data and other dynamic complex network structures.

Yulia R. Gel is Professor in the Department of Mathematical Science at the University of Texas at Dallas. Her research interests include statistical foundation of Data Science, inference for random graphs and complex networks, time series analysis and predictive analytics. She holds a Ph.D in Mathematics, followed by a postdoctoral position in Statistics at the University of Washington. Prior to joining UT Dallas, she was a tenured faculty member at the University of Waterloo, Canada. She held visiting positions at Johns Hopkins University, University of California, Berkeley, and the Isaac Newton Institute for Mathematical Sciences, Cambridge University, UK. She is Fellow of the American Statistical Association.

Jie Zhang received the B.S. and M.S. degrees in mechanical engineering from the Huazhong University of Science and Technology, Wuhan, China, in 2006 and 2008, respectively, and the Ph.D. degree in mechanical engineering from Rensselaer Polytechnic Institute, Troy, NY, USA, in 2012. He is currently an Assistant Professor with the Department of Mechanical Engineering, University of Texas at Dallas, Dallas, TX, USA. His research interests include multidisciplinary design optimization, complex engineered systems, big data analytics, wind and solar forecasting, renewable integration, and energy systems modeling and simulation.

References

Albert, R., Albert, I., & Nakarado, G. L. (2004). Structural vulnerability of the North American power grid. *Physical Review E*, *69*(2), 025103.

Allan, R. N. (2013). *Reliability evaluation of power systems*. New York, NY: Springer Science & Business Media.

Birchfield, A. B., Xu, T., Gegner, K. M., Shetye, K. S., & Overbye, T. J. (2017). Grid structural characteristics as validation criteria for synthetic networks. *IEEE Transactions on Power Systems*, *32*(4), 3258–3265.

Calafiore, G. C., & El Ghaoui, L. (2014). *Optimization models*. Cambridge: Cambridge University Press.

Carlsson, G. (2009). Topology and data. *Bulletin of the American Mathematical Society*, *46*(2), 255–308.

Carrión, M., & Arroyo, J. M. (2006). A computationally efficient mixed-integer linear formulation for the thermal unit commitment problem. *IEEE Transactions on Power Systems*, *21*(3), 1371–1378.

Čaušević, S., Saxena, K., Warnier, M., Abhyankar, A. R., & Brazier, F. M. (2019). Energy resilience through self-organization during widespread power outages. *Sustainable and Resilient Infrastructure*, 1–15.

Chandramowli, S. N., & Felder, F. A. (2014). Impact of climate change on electricity systems and markets–A review of models and forecasts. *Sustainable Energy Technologies and Assessments*, *5*, 62–74.

Chassin, D. P., & Posse, C. (2005). Evaluating North American electric grid reliability using the Barabási–Albert network model. *Physica A: Statistical Mechanics and Its Applications*, *355*(2–4), 667–677.

Cuadra, L., Salcedo-Sanz, S., Del Ser, J., Jiménez-Fernández, S., & Geem, Z. W. (2015). A critical review of robustness in power grids using complex networks concepts. *Energies*, *8*(9), 9211–9265.

Delfinado, C., & Edelsbrunner, H. (1995). An incremental algorithm for betti numbers of simplicial complexes on the 3-sphere. *Computer Aided Geometric Design*, *12*(7), 771–784.

Ezzeldin, M., & El-Dakhakhni, W. E. (2019). Robustness of ontario power network under systemic risks. *Sustainable and Resilient Infrastructure*, 1–20.

Fang, Y.-P., Pedroni, N., & Zio, E. (2014). Comparing network-centric and power flow models for the optimal allocation of link capacities in a cascade-resilient power transmission network. *IEEE Systems Journal*, *11*(3), 1632–1643.

Gasser, P., Lustenberger, P., Cinelli, M., Kim, W., Spada, M., Burgherr, P., Hirschberg S, Stojadinovic B, & Sun, T. Y.

(2019). A review on resilience assessment of energy systems. *Sustainable and Resilient Infrastructure*, 1–27.

Ghrist, R. (2008). Barcodes: The persistent topology of data. *Bulletin of the American Mathematical Society*, *45*(1), 61–75.

Guidotti, R., Chmielewski, H., Unnikrishnan, V., Gardoni, P., McAllister, T., & van de Lindt, J. (2016). Modeling the resilience of critical infrastructure: The role of network dependencies. *Sustainable and Resilient Infrastructure*, *1* (3–4), 153–168.

Holmgren, Å. J. (2006). Using graph models to analyze the vulnerability of electric power networks. *Risk Analysis*, *26* (4), 955–969.

Islambekov, U., Dey, A., Gel, Y., & Poor, H. (2018). *Role of local geometry in robustness of power grid networks*. In Global conference on signal and information processing (globalsip), 2018 IEEE. Anaheim, CA: IEEE.

Ji, C., Wei, Y., Mei, H., Calzada, J., Carey, M., & Church, S., others. (2016). Large-scale data analysis of power grid resilience across multiple us service regions. *Nature Energy*, *1* (5), 16052.

Kerber, M., Morozov, D., & Nigmetov, A. (2016). *Geometry helps to compare persistence diagrams*. In Proceedings of the 18th workshop on algorithm engineering and experiments (alenex) (pp. 103–112). Arlington, VA: SIAM.

Kim, D. H., Eisenberg, D. A., Chun, Y. H., & Park, J. (2017). Network topology and resilience analysis of South Korean power grid. *Physica A: Statistical Mechanics and Its Applications*, *465*, 13–24.

Liu, X., Shahidehpour, M., Li, Z., Liu, X., Cao, Y., & Bie, Z. (2016). Microgrids for enhancing the power grid resilience in extreme conditions. *IEEE Transactions on Smart Grid*, *8* (2), 589–597.

National Academies of Sciences, E., & Medicine. (2017). *Enhancing the resilience of the nation's electricity system*. Washington, DC: The National Academies Press.

North American Electric Reliability Corporation. (2018). *Probabilistic adequacy and measures, technical reference report final* (Tech. Rep.). Atlanta, GA: North American Electric Reliability Corporation.

Ofori-Boateng, D., Dey, A. K., Gel, Y. R., Li, B., Zhang, J., & Poor, H. V. (2019, June). *Assessing the resilience of the Texas power grid network*. In 2019 IEEE data science workshop (dsw) (pp. 280–284). Minneapolis, MN: IEEE Signal Processing Society.

Ofori-Boateng, D., Dey, K. A., Gel, Y. R., & Poor, H. V. (n.d.). Graph-theoretic analysis of power grid robustness. Manuscript submitted for publication

Otter, N., Porter, M. A., Tillmann, U., Grindrod, P., & Harrington, H. A. (2017). A roadmap for the computation of persistent homology. *EPJ Data Science*, *6*(1), 17–17.

Ouyang, M., & Duenas-Osorio, L. (2014). Multi-dimensional hurricane resilience assessment of electric power systems. *Structural Safety*, *48*, 15–24.

Pagani, G. A., & Aiello, M. (2013). The power grid as a complex network: A survey. *Physica A: Statistical Mechanics and Its Applications*, *392*(11), 2688–2700.

Rocchetta, R., Zio, E., & Patelli, E. (2018). A power-flow emulator approach for resilience assessment of repairable power grids subject to weather-induced failures and data deficiency. *Applied Energy*, *210*, 339–350.

Rosato, V., Bologna, S., & Tiriticco, F. (2007). Topological properties of high-voltage electrical transmission networks. *Electric Power Systems Research*, *77*(2), 99–105.

Rueda, D. F., Calle, E., & Marzo, J. L. (2017, Apr 01). Robustness comparison of 15 real telecommunication networks: Structural and centrality measurements. *Journal of Network and Systems Management*, *25*(2), 269–289.

Sharma, N., Tabandeh, A., & Gardoni, P. (2018). Resilience analysis: A mathematical formulation to model resilience of engineering systems. *Sustainable and Resilient Infrastructure*, *3*(2), 49–67.

Trakas, D. N., & Hatziargyriou, N. D. (2017). Optimal distribution system operation for enhancing resilience against wildfires. *IEEE Transactions on Power Systems*, *33*(2), 2260–2271.

Wang, S., Lv, W., Zhao, L., Nie, S., & Stanley, H. (2019). Structural and functional robustness of networked critical infrastructure systems under different failure scenarios. *Physica A: Statistical Mechanics and Its Applications*, *523*, 476–487.

Wang, Y., Chen, C., Wang, J., & Baldick, R. (2016, March). Research on resilience of power systems under natural disasters–A review. *IEEE Transactions on Power Systems*, *31*(2), 1604–1613.

Wasserman, L. (2018). Topological data analysis. *Annual Review of Statistics and Its Application*, *5*(1), 501–532.

Wilbanks, T. J., & Kates, R. W. (2010). Beyond adapting to climate change: Embedding adaptation in responses to multiple threats and stresses. *Annals of the Association of American Geographers*, *100*(4), 719–728.

Willis, H. H., & Loa, K. (2015). *Measuring the resilience of energy distribution systems*. Santa Monica, CA, USA: RAND Corporation.

Wood, A. J., & Wollenberg, B. F. (2012). *Power generation, operation, and control*. Hoboken, NJ: John Wiley & Sons.

Zimmerman, R. D., Murillo-Sánchez, C. E., & Thomas, R. J. (2010). Matpower: Steady-state operations, planning, and analysis tools for power systems research and education. *IEEE Transactions on Power Systems*, *26*(1), 12–19.

Zomorodian, A. (2010). Fast construction of the vietoris-rips complex. *Computers and Graphics*, *34*(3), 263–271.